Original Article

Cardiac cine with compressed sensing real-time imaging and retrospective motion correction for free-breathing assessment of left ventricular function and strain in clinical practice

Yanyu Li[1#], Lu Lin[1#], Jian Wang[1], Likun Cao[1], Yajing Liu[1], Jianing Pang[2], Jing An[3], Zhengyu Jin[1], Yining Wang[1]

[1]Department of Radiology, State Key Laboratory of Complex Severe and Rare Diseases, Peking Union Medical College Hospital, Chinese Academy of Medical Sciences and Peking Union Medical College, Beijing, China; [2]Siemens Medical Solutions USA Inc., Chicago, IL, USA; [3]Siemens Shenzhen Magnetic Resonance Ltd., Shenzhen, China

Contributions: (I) Conception and design: Y Wang, Z Jin; (II) Administrative support: Y Wang; (III) Provision of study materials or patients: Y Wang, Z Jin; (IV) Collection and assembly of data: Y Li, L Lin; J Wang, L Cao, Y Liu; (V) Data analysis and interpretation: Y Li, L Lin; (VI) Manuscript writing: All authors; (VII) Final approval of manuscript: All authors.

[#]These authors contributed equally to this work.

Correspondence to: Yining Wang. Department of Radiology, State Key Laboratory of Complex Severe and Rare Diseases, Peking Union Medical College Hospital, Chinese Academy of Medical Sciences and Peking Union Medical College, No. 1, Shuaifuyuan, Dongcheng District, Beijing 100730, China. Email: wangyining@pumch.cn.

Background: Free-breathing cardiac cine magnetic resonance imaging (MRI) comparable to the traditional breath-hold 2D segmented cine imaging (SegBH) is clinically required for cardiac function and strain analysis. This study is to assess the feasibility and accuracy of a free-breathing cardiac cine technique (RTCSCineMoCo) combined with highly accelerated real-time acquisition, compressed sensing, and fully automated non-rigid motion correction for left ventricular (LV) function and strain analysis, using SegBH as the reference and comparing with free-breathing single-shot real-time compressed sensing cine imaging (RTCSCine) without motion correction.

Methods: A total of 67 patients scheduled for clinical cardiac MRI were included. Cine images were acquired using three techniques (SegBH, RTCSCineMoCo, RTCSCine) consecutively at 3.0 T. LV functional parameters, including ejection fraction (EF), end-diastolic volume (EDV), end-systolic volume (ESV), stroke volumes (SV), and LV mass (LVM) were measured and compared. Strain parameters including global radial (GRS), circumferential (GCS), and longitudinal (GLS) strain as well as corresponding time to peak strain (TPS) were computed by magnetic resonance (MR) feature tracking and compared. Subgroup analyses were performed according to heart rate (HR), left ventricular ejection fraction (LVEF), and etiology.

Results: All quantitative parameters of LV function and strain measured by RTCSCineMoCo ($r \geq 0.766$) and RTCSCine ($r \geq 0.712$) showed strong correlations with SegBH (all $P<0.001$). LV functional parameters were not statistically different between RTCSCineMoCo and SegBH (all $P>0.05$), but an overestimation of LV end-systolic volume (LVESV) and underestimation of LVEF and LVM were observed using RTCSCine (all $P<0.001$). GRS, GCS, and GLS by RTCSCineMoCo and RTCSCine were significantly different than those by SegBH (all $P<0.05$). All TPS values by RTCSCineMoCo showed no significant differences (all $P>0.05$) compared with SegBH, but TPS in longitudinal directions (TPSL) by RTCSCine was significantly different ($P=0.011$). There were no significant differences for GRS or GCS between RTCSCineMoCo and SegBH in patients with HR <70 bpm or LVEF <50%. GRS by RTCSCineMoCo showed similar results compared to SegBH in patients with pulmonary hypertension.

Conclusions: RTCSCineMoCo is a promising method for robust free-breathing cardiac cine

imaging, yielding more precise quantitative analytic results for LV function compared with RTCSCine. RTCSCineMoCo mildly underestimated GRS, GCS, and GLS, but showed smaller bias compared to RTCSCine in LV strain analysis.

Keywords: Left ventricle; cine; compressed sensing; free-breathing; strain

Submitted Jun 13, 2022. Accepted for publication Feb 07, 2023. Published online Mar 01, 2023.
doi: 10.21037/qims-22-596
View this article at: https://dx.doi.org/10.21037/qims-22-596

Introduction

Cardiac magnetic resonance (CMR) cine imaging is an attractive and comprehensive method to accurately assess ventricular function and dynamically display ventricle wall movement. Currently, CMR cine imaging is the gold standard for evaluating left ventricular (LV) volumes, mass (LVM), and ejection fraction (LVEF). Myocardial strain is an incremental technique to evaluate ventricle deformation, which can detect early-stage ventricular dysfunction when ejection fraction (EF) is preserved (1-3). CMR-feature tracking (CMR-FT) is based on conventional cine imaging to evaluate myocardial strain. Recently, CMR-FT was used for early identification of numerous cardiac diseases including ischemic cardiomyopathy (4,5), non-ischemic cardiomyopathy (6), pulmonary arterial hypertension (7), and myocarditis (8).

Currently, breath-hold 2D segmented cine imaging (SegBH) is the non-invasive standard method used to assess cardiac function (9). However, it requires multiple breath-hold to acquire cine images, which results in a long scan time and reduced image quality when patients have difficulty holding their breath. Real-time imaging has the potential to reduce respiratory motion artifacts by acquiring data of each cardiac phase in a single shot, enables shorter breath-hold times or fully free-breathing imaging, but sacrifices spatiotemporal resolution. Compressed sensing is an emergent technique playing a pivotal role in CMR acquisition acceleration comprehensively, covering cine imaging (10,11), late gadolinium enhancement imaging (12,13), and magnetic resonance (MR) angiography (14,15). Recently, real-time cine imaging with compressed sensing (RTCSCine) was used to acquire cine images during free breathing. Several studies demonstrated that RTCSCine compromised cine image quality and LV function parameters compared with SegBH (16,17), but statistically significant differences remained in some volumetric parameters and further technical improvement is needed. Additionally, few studies have examined the value of RTCSCine in myocardial strain evaluations.

In this study, we aimed to assess the feasibility and accuracy of a prototype free-breathing cardiac cine MR imaging (MRI) (RTCSCineMoCo) with highly accelerated real-time acquisition, compressed sensing, and fully automated non-rigid motion correction (18) for LV function and strain analysis. SegBH was used as a reference standard and compared with RTCSCine without motion correction.

Methods

Study population

This study included 71 patients evaluated in our department from October 2020 to April 2021. The exclusion criteria were any general contraindications to MRI (such as cardiac implantable electronic device or claustrophobia, n=3) and refusal to participate (n=1). With that, 67 subjects were prospectively studied. All participants were scheduled to undergo three cine sequences, including SegBH (the reference method), RTCSCineMoCo, and RTCSCine. The study was conducted in accordance with the Declaration of Helsinki (as revised in 2013). The study protocol was approved by the local institutional review board (No. JS-2658). All participants provided written informed consent.

Cine imaging protocol and sequences

All CMR examinations were performed on a clinical 3T MR scanner (MAGNETOM Skyra; Siemens Healthcare, Erlangen, Germany) with an 18-channel body matrix coil and 32-channel spine matrix coil. Based on the typical, localized images, the cardiac axis views were planned, including three long axes (four-chamber, three-chamber, two-chamber) and a stack of 8 to 12 short-axis slices covering the entire LV from mitral valve to apex. After that, cine imaging was performed sequentially for all three long

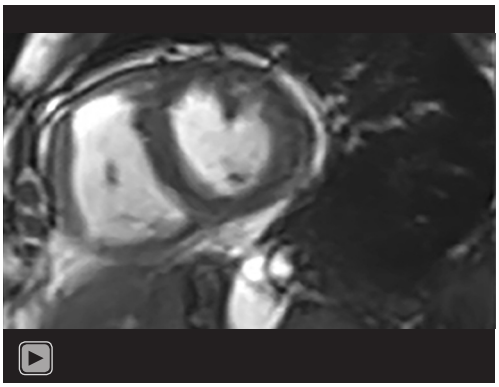

Video 1 Dynamic cine images derived from SegBH of a 69-year-old woman with pulmonary arterial hypertension and prominent breath-hold impairment. SegBH, segmented acquisition with retrospective electrocardiogram gating and breath-hold.

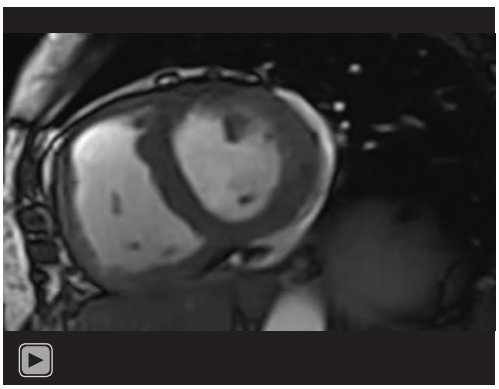

Video 2 Dynamic cine images derived from RTCSCineMoCo of the same patients in *Video 1*. RTCSCineMoCo, real-time cine imaging combines compressed sensing reconstruction and retrospective fully automated respiratory motion correction.

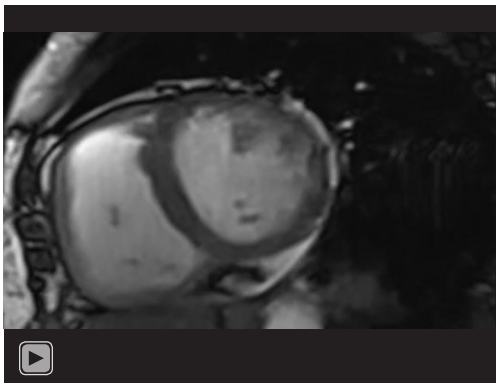

Video 3 Dynamic cine images derived from RTCSCine of the same patients in *Video 1*. RTCSCine, real-time cine imaging with compressed sensing.

axis and short-axis slices before the application of contrast agent using three techniques (SegBH, RTCSCineMoCo, and RTCSCine). Retrospectively electrocardiogram (ECG)-gated SegBH was initially performed with breath-hold at the end of expiration [repetition time (TR)/echo time (TE): 3.3/1.4 ms; temporal resolution: 45 ms (interpolated to 25 cardiac phases); field of view: 340 mm × 265 mm; spatial resolution: 1.6×1.6–1.8×1.8 mm^2; slice thickness: 8 mm; gap: 2 mm; flip angle (FA): 50°–70°; bandwidth: 962 Hz/pixel; acceleration factor: Generalized Autocalibrating Partially Parallel Acquisition (GRAPPA) 3], and then adaptively ECG-triggered RTCSCineMoCo (TR/TE: 3.2/1.4 ms; temporal resolution: RR interval/25; field of view: 340 mm × 276 mm; spatial resolution: 1.8×1.8 mm^2; slice thickness: 8 mm; gap: 2 mm; FA: 40°–50°; bandwidth: 930 Hz/pixel; acceleration factor: compressed sensing 9.9–17.3) and RTCSCine (TR/TE: 3.2/1.4 ms; temporal resolution: RR interval/25; field of view: 340 mm × 276 mm; spatial resolution: 1.8×1.8 mm^2; slice thickness: 8 mm; gap: 2 mm; FA: 40°–50°; bandwidth: 920 Hz/pixel; acceleration factor: compressed sensing 9.9–17.3) were performed while free breathing (Figure S1 and *Videos 1-3*). The total scan time of each technique was recorded.

Both of RTCSCineMoCo and RTCSCine used real-time cardiac cine sequence with incoherent Cartesian k-space sampling and balanced steady-state free precession (bSSFP) readout (10,19) for image acquisition. For RTCSCineMoCo, the data was acquired over 12 heartbeats in order to sufficiently cover multiple respiratory cycles. Every k-space line was then rebinned based on the trigger time to ensure each heartbeat has the same number of cardiac phases, which was necessary for motion correction. After this beat-to-beat normalization, real-time cine frames were reconstructed by jointly using iterative reconstruction with redundant Haar wavelets for spatiotemporal regularization (10,19). After all the heartbeats were reconstructed, the images were ranked according to the presence of respiratory motion and other attributes such as arrhythmia. This was done by calculating a motion score defined as the sum of pixel-wise absolute difference between the first and last image frame of each heartbeat:

$$Score\ of\ beat = \sum_{All\ pixels} |First\ frame\ of\ beat - Last\ frame\ of\ beat| \quad [1]$$

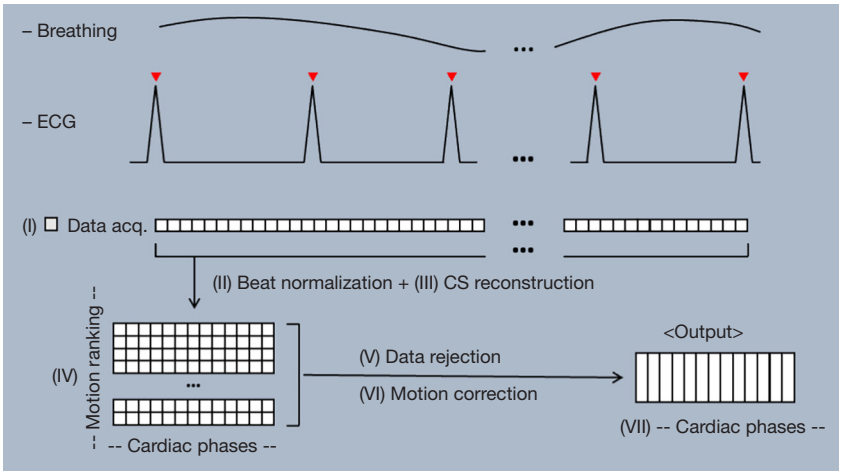

Figure 1 The RTCSCineMoCo acquisition and reconstruction workflow consists of the following steps: (I) acquiring real-time cine data over multiple heartbeats; (II) normalizing each acquired heartbeat into a protocol-defined number of cardiac phases; (III) reconstructing real-time cine frames via compressed sensing reconstruction; (IV) ranking the acquired heartbeats by detected respiratory motion and presence of arrhythmia; (V) selecting a subset of heartbeats based on ranking; (VI) registering the selected heartbeats to the top ranked reference heartbeat via non-rigid registration; (VII) computing the average of the registered heartbeats as the output. ECG, electrocardiogram; CS, compressed sensing.

The lower the score is for a given heartbeat, the more similar the first and last cine frames are, and, based on our hypothesis, the less non-cardiac motion the heartbeat experiences. Therefore, the heartbeat with the lowest score was selected as the reference for subsequent motion correction. After calculating the motion scores, a subset (typically around one third) of the acquired heartbeats with the lowest scores were selected for further processing. For additional robustness, time-based arrhythmia rejection was performed by rejecting those heartbeats with RR durations outside of a predefined range, typically plus and minus two standard deviations (SDs), around the median RR duration. Finally, each cardiac phase in each selected heartbeat was registered with the corresponding cardiac phase in the reference beat by non-rigid registration (20), and then the average of all registered heartbeats was computed as the final output. The schematic diagram of RTCSCineMoCo sequence was shown in *Figure 1*. RTCSCine used data from one RR interval to reconstruct whole image phases for each slice without motion correction and signal average, the other parameters were identical to RTCSCineMoCo.

Image analysis

All cine images were assessed by two experienced radiologists (L Lin and Y Li, with 10 and 3 years of cardiovascular MRI experience, respectively) independently using a five-point Likert scale for image quality: 5 = excellent image quality, 4 = normal image quality, 3 = presence of artifacts but sufficient image quality, 2 = severe artifacts around ventricles, and 1 = complete non-diagnostic images. Datasets with a score >2 for SegBH were included in the study (10). Any disagreements were resolved by discussion. Dedicated software was used for all cardiovascular MRI analyses (cvi42, version 5.13; Circle Cardiovascular Imaging Inc., Calgary, Canada) to assess quantitative parameters. All contours used for functional and strain analyses were firstly automatically generated, then further reviewed and corrected by experienced radiologists. LV volume and LVM analyses were based on short-axis view cine MRI and calculated using the Simpson method. The contouring of the LV endocardial and epicardial borders in end-diastole and end-systole for three cine CMR images followed the recommendations of the Society for Cardiovascular Magnetic Resonance for post-processing (21). The LV myocardial strain values were calculated using a stack of short-axis and three long-axis by MR feature tracking (*Figure 2*). The endocardial and epicardial borders in the LV end-diastole phase were chosen, and the borders for subsequent phase imaging were automatically created. Global strain values and time to peak strain (TPS) values were recorded. In addition, LV volume

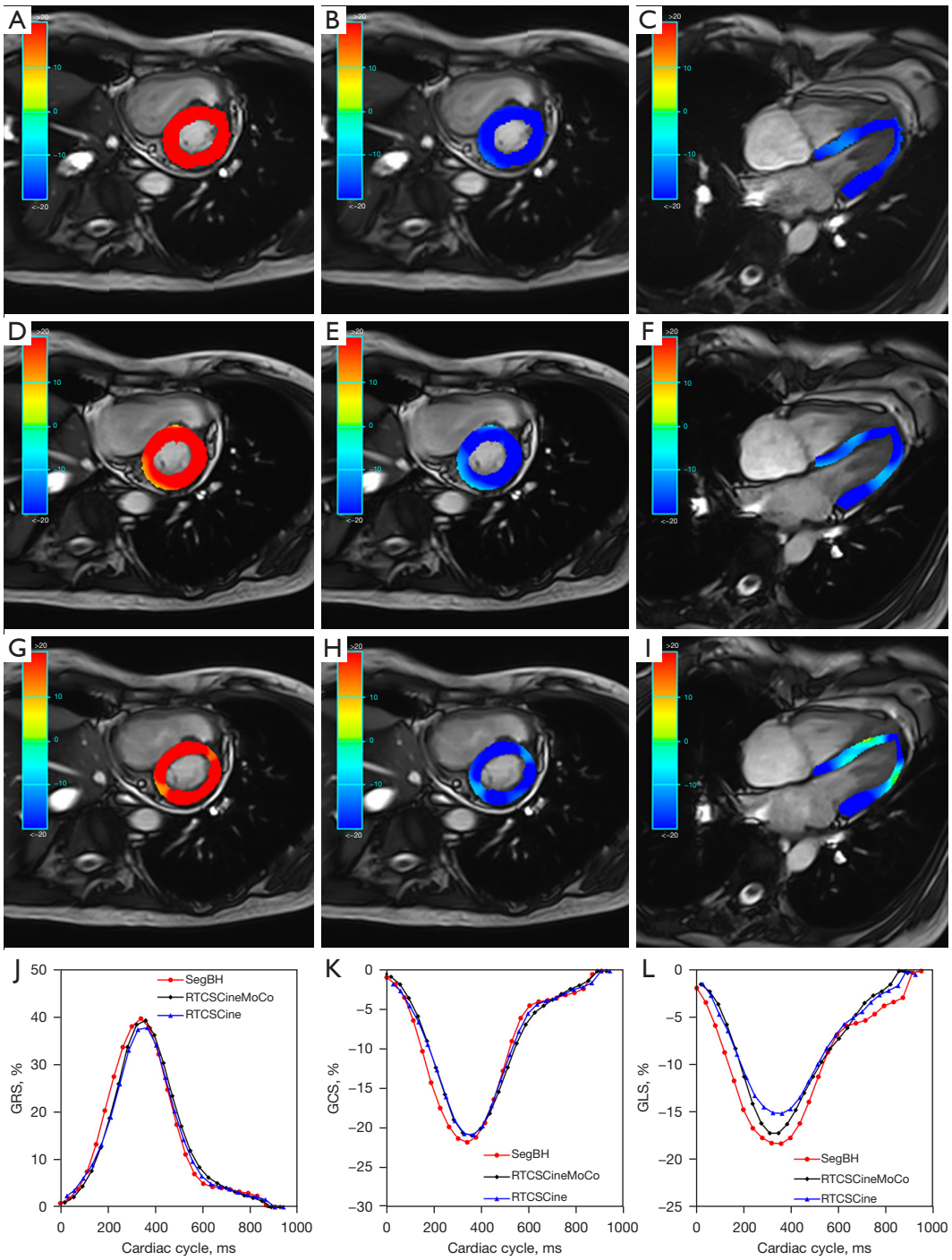

Figure 2 A 30-year-old woman (LVEF: 65.8%; HR: 67 bpm) with myocarditis. Images acquired by SegBH (A-C), RTCSCineMoCo (D-F), and RTCSCine (G-I). The GRS, GCS, and GLS are shown from left to right with the following measurements: SegBH: GRS =39.79%, GCS =−21.67%, GLS =−18.2%. RTCSCineMoCo: GRS =39.35%, GCS =−20.81%, GLS =−17.1%. RTCSCine: GRS =37.83%, GCS =−20.75%, GLS =−15.02%. Bottom row: strain curves of GRS, GCS, and GLS (J-L). GCS, global circumferential strain; GLS, global longitudinal strain; GRS, global radial strain; HR, heart rate; LVEF, left ventricular ejection fraction; RTCSCine, real-time cine imaging with compressed sensing; RTCSCineMoCo, real-time cine imaging combines compressed sensing reconstruction and retrospective fully automated respiratory motion correction; SegBH, segmented acquisition with retrospective electrocardiogram gating and breath-hold.

Table 1 Study population demographics (n=67)

Characteristic	Result
Age (years)	38±19
Men	22 [33]
Height (cm)	164.2±9.6
Weight (kg)	60±13
Body mass index (kg/m^2)	22.2±3.9
Heart rate (beats/min)	74±13
Diagnosis	
Pulmonary hypertension	32 [48]
Dilated cardiomyopathy	8 [12]
Coronary artery disease	5 [7]
Congenital heart disease	3 [4]
Myocarditis	2 [3]
Left ventricular noncompaction	2 [3]
Cardiac amyloidosis	2 [3]
Connective tissue disease	13 [19]

Data are mean ± standard deviation or number [percentage].

and global LV myocardial strain were assessed in subgroups according to heart rate (HR), LVEF, and etiology. Subjects were stratified by HR (lower HR group, <70 bpm; higher HR group, ≥70 bpm), by LVEF (reduced LVEF, <50%; normal LVEF, ≥50%) measured by SegBH and by etiology [patients with or without pulmonary hypertension (PH)].

Reproducibility

Intra-observer reproducibility was assessed in 20 randomly selected patients for each technique with a time interval of two weeks between analyses (Y Li). Inter-observer variability was assessed in the same 20 patients by comparing the results from the two independent observers (L Lin and Y Li).

Statistical analysis

Continuous variables are presented as mean and SD in the case of normal distribution and median (25th–75th percentile), otherwise. Categorical variables are presented as frequency and percentage. The LV structure and function were measured quantitatively and compared using Wilcoxon matched-pairs signed-rank test or paired *t*-test depending on whether the data followed a normal distribution. Linear regression analysis was utilized to assess the correlation and consistency of quantitative metrics across different techniques. Bland-Altman analysis was used to assess bias. Consistency was assessed using inter- and intra-class correlation coefficients (ICC). A P value <0.05 was considered statistically significant. All statistical analyses were performed with SPSS software (version 26.0, SPSS Inc., Chicago, IL, USA).

Results

Basic characteristics of the study population

A total of 67 subjects were included in our study, and all completed the three types of cine imaging successfully. Baseline demographic characteristics and cardiac diagnoses are shown in *Table 1*. The mean scan times were 135±39, 112±20, and 19±3 s, respectively for SegBH, RTCSCineMoCo, and RTCSCine. The scan times for RTCineMoCo and RTCSCine were both significantly lower than SegBH (all P<0.001). The subjective image quality scores of SegBH, RTCSCineMoCo, and RTCSCine were assessed as 4.1±0.8, 4.3±0.8, and 3.9±0.8, respectively. No significant differences were seen for image quality scores between RTCSCineMoCo and SegBH (Z=−1.397, P=0.162) or RTCSCine and SegBH (Z=−1.921, P=0.055), but RTCSCineMoCo showed significantly higher image quality scores than RTCSCine (Z=−3.704, P<0.001).

Quantitative LV functional analyses

All LV functional parameters measured by three different techniques are shown in *Table 2*. There were no statistical differences between RTCSCineMoCo and SegBH for LV functional parameters, including LVEF (P=0.837), LV end-diastolic volume (LVEDV, P=0.164), LV end-systolic volume (LVESV, P=0.587), LV stroke volumes (LVSV, P=0.163), and LVM (P=0.457). No statistical differences were observed between RTCSCine and SegBH for LVEDV (P=0.283), and LVSV (P=0.058) measurements, but significant overestimation of LVESV (59.0±38.0 *vs.* 56.2±37.1, P<0.001), and underestimation of LVEF (55.6±13.1 *vs.* 57.4±13.7, P<0.001) and LVM (85.8±33.9 *vs.* 91.2±32.0, P<0.001) were observed between RTCSCine and SegBH. Detailed values are listed in *Table 2*. Linear regression and Bland-Altman analyses showed a stronger

Table 2 Quantitative measures of LV function and strain

Parameters	SegBH, mean ± SD	RTCSCineMoCo			RTCSCine		
		Mean ± SD	P value*	r	Mean ± SD	P value*	r
LVEF (%)	57.4±13.7	57.3±13.1	0.837	0.985	55.6±13.1	<0.001‡	0.963
LVEDV (mL)	125.0±46.7	126.1±45.9	0.164	0.992	126.2±47.1	0.283	0.984
LVESV (mL)	56.2±37.1	56.5±36.4	0.587	0.995	59.0±38.0	<0.001‡	0.991
LVSV (mL)	68.8±23.5	69.6±22.9	0.163	0.983	67.2±22.6	0.058	0.953
LVM (g)	91.2±32.0	90.7±33.2	0.457	0.987	85.8±33.9	<0.001‡	0.946
GRS (%)	29.0±11.4	27.9±10.4	0.022†	0.944	26.3±10.1	<0.001‡	0.917
GCS (%)	−17.0±4.8	−16.2±4.3	<0.001†	0.952	−15.4±4.3	<0.001‡	0.922
GLS (%)	−15.8±4.0	−11.7±3.9	<0.001†	0.803	−10.2±2.9	<0.001‡	0.712
TPS_R (ms)	303.8±42.2	300.4±45.7	0.348	0.785	299.1±43.6	0.175	0.789
TPS_C (ms)	303.4±42.8	299.9±45.9	0.308	0.808	299.5±44.6	0.308	0.750
TPS_L (ms)	317.4±53.8	306.6±55.6	0.114	0.766	305.0±55.8	0.011‡	0.753

Measurements of RTCSCineMoCo and RTCSCine were analyzed using SegBH as a reference standard. *, P values were obtained by paired *t*-test; †, P<0.05, RTCSCineMoCo versus SegBH; ‡, P<0.05, RTCSCine versus SegBH. GCS, global circumferential strain; GLS, global longitudinal strain; GRS, global radial strain; LV, left ventricular; LVEDV, left ventricular end-diastolic volume; LVEF, left ventricular ejection fraction; LVESV, left ventricular end-systolic volume; LVM, left ventricular mass; LVSV, left ventricular stroke volume; r, correlation coefficient; RTCSCine, real-time cine imaging with compressed sensing; RTCSCineMoCo, real-time cine imaging combines compressed sensing reconstruction and retrospective fully automated respiratory motion correction; SD, standard deviation; SegBH, segmented acquisition with retrospective electrocardiogram gating and breath-hold; TPS_C, time to peak strain in circumferential; TPS_L, time to peak strain in longitudinal; TPS_R, time to peak strain in radial.

correlation and smaller bias for all LV volume parameters between RTCSCineMoCo and SegBH than between RTCSCine and SegBH (*Figure 3*). All parameters for each technique demonstrated good inter-observer and intra-observer agreement; corresponding ICC values are provided in *Table 3*.

Quantitative LV strain analyses

Global radial strain (GRS), global circumferential strain (GCS), and global longitudinal strain (GLS) derived from RTCSCineMoCo or RTCSCine were significantly lower than those derived from SegBH. The mean values of GRS, GCS, and GLS obtained from the standard SegBH sequence were 29.0±11.4, −17.0±4.8, and −15.8±4.0, respectively. The corresponding values were 27.9±10.4, −16.2±4.3, and −11.7±3.9, respectively for RTCSCineMoCo and 26.3±10.1, −15.4±4.3, and −10.2±2.9, respectively for RTCSCine (*Table 2*). GRS, GCS, and GLS obtained from RTCSCineMoCo and RTCSCine were significantly correlated with those from SegBH (r=0.944, r=0.952, and r=0.803 for RTCSCineMoCo; r=0.917, r=0.922, and r=0.712 for RTCSCine respectively). For Bland-Altman analyses, all measurements derived from RTCSCineMoCo and SegBH showed smaller bias and narrower 95% confidence interval (CI) than RTCSCine and SegBH (*Figure 4*). The values of TPS in the radial (TPS_R), circumferential (TPS_C), and longitudinal (TPS_L) directions were not significantly different between RTCSCineMoCo and SegBH, but TPSL obtained from RTCSCine was slightly lower than SegBH (305.0±55.8 *vs.* 317.4±53.8, P=0.011) (*Figure 5*). In the linear regression analysis, r values derived from RTCSCineMoCo and SegBH were higher than from RTCSCine and SegBH except for TPS_R (*Table 2*, *Figure 4*). All strain parameters for each technique demonstrated good inter-observer and intra-observer agreement; corresponding ICC values are provided in *Table 3*.

Subgroup quantitative analyses according to HR, LVEF, and etiology

Compared with SegBH, RTCSCineMoCo acquired similar

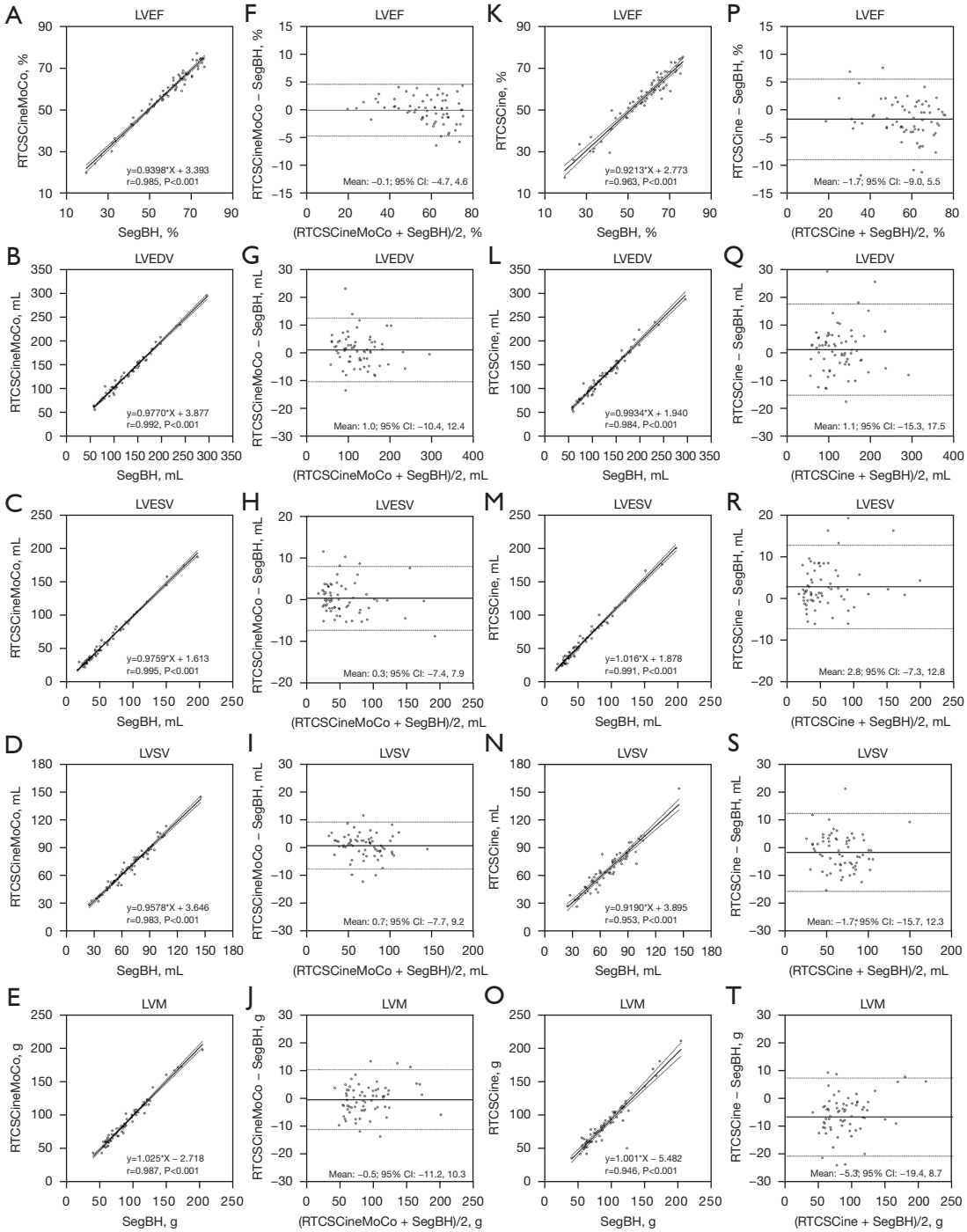

Figure 3 Linear regression analysis and Bland-Altman plots between RTCSCineMoCo and SegBH (A-J) and between RTCSCine and SegBH (K-T) for LV functional parameters including LVEF, LVEDV, LVESV, LVSV, and LVM. (—) Mean difference; (---) 95% CI limits of agreement. CI, confidence interval; LV, left ventricular; LVEDV, left ventricular end-diastolic volume; LVEF, left ventricular ejection fraction; LVESV, left ventricular end-systolic volume; LVM, left ventricular mass; LVSV, left ventricular stroke volume; r, correlation coefficient; RTCSCine, real-time cine imaging with compressed sensing; RTCSCineMoCo, real-time cine imaging combines compressed sensing reconstruction and retrospective fully automated respiratory motion correction; SegBH, segmented acquisition with retrospective electrocardiogram gating and breath-hold.

Table 3 ICCs of intra- and inter-observer agreement

Parameter	SegBH		RTCSCineMoCo		RTCSCine	
	Inter-observer	Intra-observer	Inter-observer	Intra-observer	Inter-observer	Intra-observer
LVEF (%)	0.971	0.994	0.982	0.955	0.965	0.974
LVEDV (mL)	0.992	0.994	0.994	0.998	0.994	0.994
LVESV (mL)	0.992	0.998	0.996	0.994	0.990	0.989
LVSV (mL)	0.979	0.984	0.984	0.984	0.986	0.983
LVM (g)	0.989	0.985	0.962	0.966	0.902	0.997
GRS (%)	0.976	0.992	0.985	0.931	0.966	0.968
GCS (%)	0.981	0.993	0.978	0.933	0.972	0.975
GLS (%)	0.972	0.989	0.844	0.923	0.783	0.891
TPS_R (ms)	0.840	0.999	0.926	0.925	0.971	0.836
TPS_C (ms)	0.885	0.999	0.926	0.925	0.841	0.890
TPS_L (ms)	0.895	0.993	0.797	0.843	0.874	0.897

ICCs, intraclass correlation coefficients; GCS, global circumferential strain; GLS, global longitudinal strain; GRS, global radial strain; ICC, intraclass correlation coefficient; LV, left ventricular; LVEDV, left ventricular end-diastolic volume; LVEF, left ventricular ejection fraction; LVESV, left ventricular end-systolic volume; LVM, left ventricular mass; LVSV, left ventricular stroke volume; RTCSCine, real-time cine imaging with compressed sensing; RTCSCineMoCo, real-time cine imaging combines compressed sensing reconstruction and retrospective fully automated respiratory motion correction; SegBH, segmented acquisition with retrospective electrocardiogram gating and breath-hold; TPS_C, time to peak strain in circumferential; TPS_L, time to peak strain in longitudinal; TPS_R, time to peak strain in radial.

results for most LV functional parameters in subgroups according to HR, LVEF, and etiology, except for slightly higher LVEDV values in the HR <70 bpm subgroup (130.2±44.5 *vs.* 127.2±45.6, P=0.026) and LVEF values in the LVEF <50% subgroup (38.9±9.3 *vs.* 37.8±9.1, P=0.010). Correspondingly, RTCSCine acquired similar results of LV functional analyses in the LVEF <50% subgroup, but in the other subgroups, most of the results showed significant differences (*Tables 4-6*, *Figure 6*).

For strain analyses, compared to SegBH, the GLS values of RTCSCineMoCo and RTCSCine were still significantly underestimated in all subgroups. But the GRS and GCS values of RTCSCineMoCo and RTCSCine showed no significant differences in the HR <70 bpm and LVEF <50% subgroup, except for GCS values of RTCSCine in the HR <70 bpm (*Tables 4,5*, *Figure 6*). GRS and GCS values of RTCSCineMoCo and RTCSCine were still underestimated in subgroups with or without PH, except for GRS values of RTCSCineMoCo in patients with PH (*Table 6*, *Figure 6*).

Discussion

In this study, we tested a prototype free-breathing cine imaging (RTCSCineMoCo) combined with extending real-time data acquisition to multiple heartbeats and performed non-rigid respiratory motion correction for LV function and strain analysis. Compared with the standard SegBH method, RTCSCineMoCo shortened scan time and achieved equivalent image quality and LV functional parameters under free breathing. Although RTCSCine shortened scan time more prominently, its image quality was impaired and LV functional measurements showed significant deviations. For LV strain analysis, both of RTCSCineMoCo and RTCSCine underestimated GRS, GLS, and GCS, but RTCSCineMoCo showed higher correlation to the results by SegBH. All TPS values by RTCSCineMoCo showed no significant differences compared with SegBH.

Several early studies have demonstrated the feasibility of applying real-time compressed sensing cine imaging techniques to accelerated cardiac cine imaging to evaluate LV volumes and function (10,22). The majority of research yielded strong agreement between compressed sensing and traditional techniques in terms of quantitative measurements, but notable differences remained in certain parameters. An early study applied real-time cine sequence using SPARSE-SENSE for LV analysis at 1.5 T in 20 patients

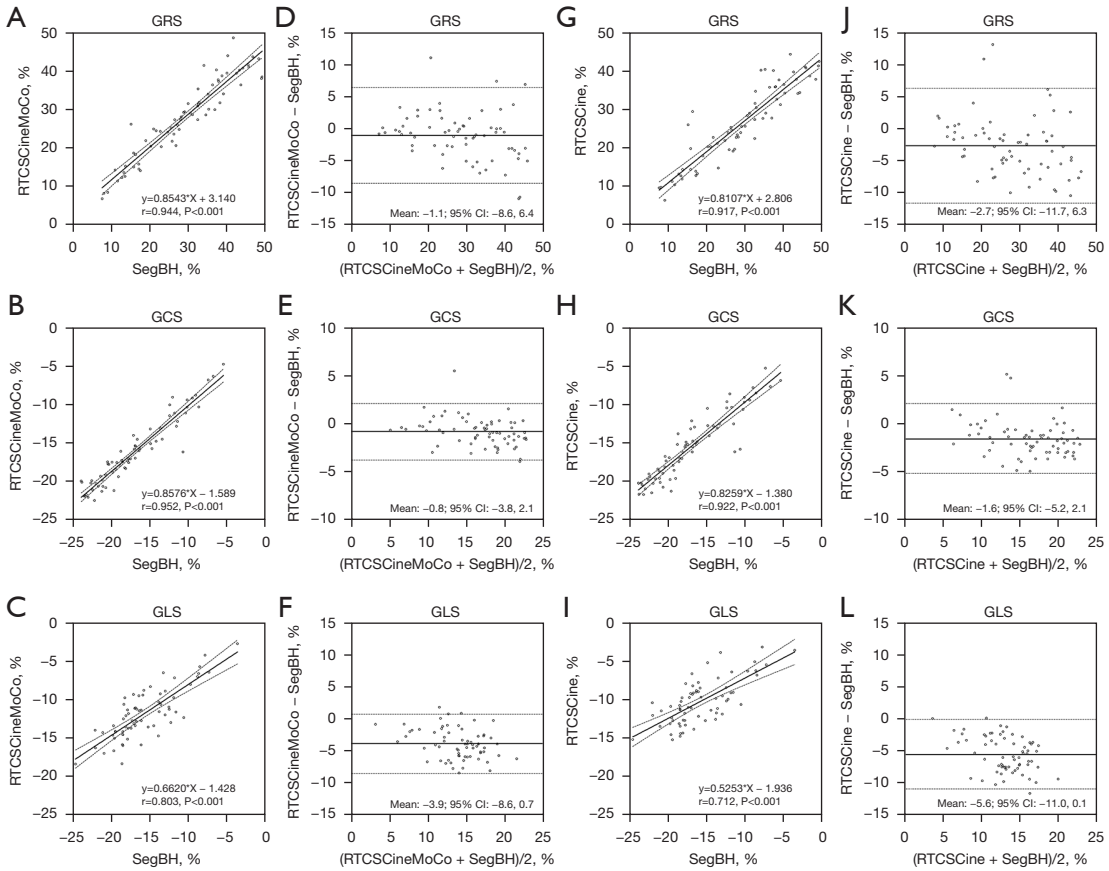

Figure 4 Linear regression analysis and Bland-Altman plots between RTCSCineMoCo and SegBH (A-F) and between RTCSCine and SegBH (G-L) for LV strain measurements. GRS, GCS, and GLS are the global strain in radial, circumferential, and longitudinal directions, respectively. (—) Mean difference; (---) 95% CI limits of agreement. GCS, global circumferential strain; GLS, global longitudinal strain; GRS, global radial strain; LV, left ventricular; r, correlation coefficient; RTCSCine, real-time cine imaging with compressed sensing; RTCSCineMoCo, real-time cine imaging combines compressed sensing reconstruction and retrospective fully automated respiratory motion correction; SegBH, segmented acquisition with retrospective electrocardiogram gating and breath-holding.

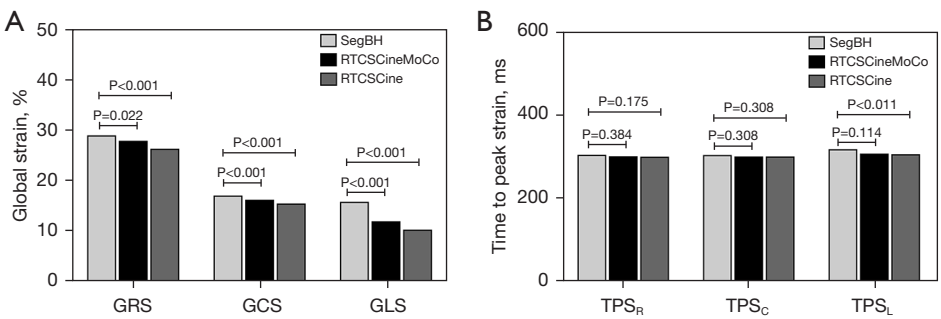

Figure 5 Comparison of global strain (A) and time to peak strain (B) between RTCSCineMoCo and SegBH and between RTCSCine and SegBH. GCS, global circumferential strain; GLS, global longitudinal strain; GRS, global radial strain; RTCSCine, real-time cine imaging with compressed sensing; RTCSCineMoCo, real-time cine imaging combines compressed sensing reconstruction and retrospective fully automated respiratory motion correction; SegBH, segmented acquisition with retrospective electrocardiogram gating and breath-hold; TPS_C, time to peak strain in circumferential; TPS_L, time to peak strain in longitudinal; TPS_R, time to peak strain in radial.

Table 4 LV quantitative measures in HR subgroups

Parameter	HR <70 bpm (n=26)					HR ≥70 bpm (n=41)				
	SegBH, mean ± SD	RTCSCineMoCo		RTCSCine		SegBH, mean ± SD	RTCSCineMoCo		RTCSCine	
		Mean ± SD	P value*	Mean ± SD	P value*		Mean ± SD	P value*	Mean ± SD	P value*
LVEF (%)	54.0±16.5	53.7±15.7	0.573	52.2±15.3	0.080	59.5±11.3	59.6±10.7	0.852	57.8±11.2	<0.001‡
LVEDV (mL)	127.2±45.6	130.2±44.5	0.026†	129.6±45.1	0.207	123.7±47.8	123.4±47.2	0.799	123.9±48.7	0.820
LVESV (mL)	62.3±41.1	63.7±41.1	0.099	65.9±42.1	0.011‡	52.3±34.2	51.9±32.8	0.431	54.6±35.0	0.001‡
LVSV (mL)	64.9±23.4	66.5±22.6	0.093	63.8±20.5	0.533	71.3±23.4	71.6±23.1	0.729	69.3±23.9	0.026‡
LVM (g)	96.9±36.3	96.2±36.9	0.577	92.0±39.0	0.010‡	87.5±28.9	87.2±30.7	0.653	81.8±30.0	0.004‡
GRS (%)	26.2±12.8	26.0±11.8	0.696	24.9±11.0	0.170	30.8±10.3	29.2±9.3	0.017†	27.2±9.5	<0.001‡
GCS (%)	−15.6±5.7	−15.2±5.2	0.050	−14.7±4.9	0.014‡	−17.9±4.0	−16.8±3.6	<0.001†	−15.9±3.8	<0.001‡
GLS (%)	−14.7±4.6	−11.3±4.1	<0.001†	−9.8±3.6	<0.001‡	−16.5±3.4	−12.2±2.6	<0.001†	−10.5±2.4	<0.001‡

*, P values were obtained by paired *t*-test; †, P<0.05, RTCSCineMoCo versus SegBH; ‡, P<0.05, RTCSCine versus SegBH. GCS, global circumferential strain; GLS, global longitudinal strain; GRS, global radial strain; HR, heart rate; LV, left ventricular; LVEDV, left ventricular end-diastolic volume; LVEF, left ventricular ejection fraction; LVESV, left ventricular end-systolic volume; LVM, left ventricular mass; LVSV, left ventricular stroke volume; RTCSCine, real-time cine imaging with compressed sensing; RTCSCineMoCo, real-time cine imaging combines compressed sensing reconstruction and retrospective fully automated respiratory motion correction; SD, standard deviation; SegBH, segmented acquisition with retrospective electrocardiogram gating and breath-hold.

Table 5 LV quantitative measures in LVEF subgroups

Parameter	LVEF <50% (n=17)					LVEF ≥50% (n=50)				
	SegBH, mean ± SD	RTCSCineMoCo		RTCSCine		SegBH, mean ± SD	RTCSCineMoCo		RTCSCine	
		Mean ± SD	P value*	Mean ± SD	P value*		Mean ± SD	P value*	Mean ± SD	P value*
LVEF (%)	37.8±9.1	38.9±9.3	0.010†	37.4±9.3	0.659	64.0±7.1	63.6±6.7	0.232	61.8±7.0	<0.001‡
LVEDV (mL)	157.1±60.6	158.0±58.9	0.535	159.1±59.3	0.265	114.2±35.4	115.2±35.2	0.219	115.0±36.5	0.526
LVESV (mL)	99.6±46.2	98.9±45.4	0.540	102.8±48.0	0.053	41.5±16.7	42.0±16.5	0.293	44.1±17.4	<0.001‡
LVSV (mL)	57.5±21.5	59.0±20.9	0.079	56.3±18.0	0.543	72.7±23.0	73.2±22.6	0.469	70.8±23.0	0.067
LVM (g)	112.0±41.7	112.0±42.6	0.986	108.2±44.0	0.053	84.1±24.7	83.4±26.2	0.411	78.1±26.0	0.001‡
GRS (%)	15.0±5.3	15.5±5.9	0.557	14.8±6.1	0.863	33.8±8.7	32.2±7.8	0.005†	30.3±8.0	<0.001‡
GCS (%)	−10.8±3.0	−10.7±3.3	0.875	−10.3±3.1	0.416	−19.1±3.2	−18.0±2.8	<0.001†	−17.2±3.1	<0.001‡
GLS (%)	−11.1±3.3	−8.9±3.2	<0.001†	−7.6±2.8	<0.001‡	−17.4±2.8	−12.9±2.6	<0.001†	−11.1±2.4	<0.001‡

*, P values were obtained by paired *t*-test; †, P<0.05, RTCSCineMoCo versus SegBH; ‡, P<0.05, RTCSCine versus SegBH. GCS, global circumferential strain; GLS, global longitudinal strain; GRS, global radial strain; LV, left ventricular; LVEDV, left ventricular end-diastolic volume; LVEF, left ventricular ejection fraction; LVESV, left ventricular end-systolic volume; LVM, left ventricular mass; LVSV, left ventricular stroke volume; RTCSCine, real-time cine imaging with compressed sensing; RTCSCineMoCo, real-time cine imaging combines compressed sensing reconstruction and retrospective fully automated respiratory motion correction; SD, standard deviation; SegBH, segmented acquisition with retrospective electrocardiogram gating and breath-hold.

with atrial fibrillation. The SPARSE-SENSE technique yielded results comparable to multi-breath-hold segmented cine for LVEF, LVEDV, LVSV, and LV mass, but significantly larger LVESV (78±48 *vs.* 70±42, P=0.019) (23). In our results, an overestimation of LVESV was found in addition to significant underestimations of LVEF and LVM when

Table 6 LV quantitative measures in etiology subgroups

Parameter	Patients with PH (n=32)					Patients without PH (n=35)				
	SegBH, mean ± SD	RTCSCineMoCo		RTCSCine		SegBH, mean ± SD	RTCSCineMoCo		RTCSCine	
		Mean ± SD	P value*	Mean ± SD	P value*		Mean ± SD	P value*	Mean ± SD	P value*
LVEF (%)	60.6±12.2	60.5±11.6	0.877	59.5±10.6	0.096	54.4±14.5	54.4±13.9	0.894	52.1±14.3	0.001‡
LVEDV (mL)	110.0±39.2	110.8±38.6	0.415	110.4±40.4	0.707	138.8±49.1	140.0±48.2	0.259	140.5±48.7	0.300
LVESV (mL)	44.2±28.4	44.9±28.5	0.282	45.9±28.7	0.025‡	67.2±40.9	67.1±39.8	0.862	71.0±41.8	<0.001‡
LVSV (mL)	65.8±23.8	66.0±22.7	0.813	64.6±22.1	0.244	71.6±23.2	72.9±22.9	0.076	69.5±23.1	0.139
LVM (g)	80.1±30.0	78.1±31.2	0.062	75.4±30.9	0.001‡	101.3±30.8	102.2±32.9	0.385	95.2±34.1	0.012‡
GRS (%)	32.2±11.7	31.4±10.1	0.330	30.1±9.1	0.044‡	26.1±10.6	24.8±9.7	0.004†	22.9±9.9	<0.001‡
GCS (%)	−18.2±4.9	−17.5±4.2	0.023†	−17.0±3.8	0.004‡	−15.9±4.5	−15.0±4.2	<0.001†	−14.0±4.3	<0.001‡
GLS (%)	−16.7±4.1	−12.5±3.6	<0.001†	−10.7±3.2	<0.001‡	−14.9±3.7	−11.3±2.9	<0.001†	−9.8±2.7	<0.001‡

*, P values were obtained by paired *t*-test; †, P<0.05, RTCSCineMoCo versus SegBH; ‡, P<0.05, RTCSCine versus SegBH. GCS, global circumferential strain; GLS, global longitudinal strain; GRS, global radial strain; LV, left ventricular; LVEDV, left ventricular end-diastolic volume; LVEF, left ventricular ejection fraction; LVESV, left ventricular end-systolic volume; LVM, left ventricular mass; LVSV, left ventricular stroke volume; PH, pulmonary hypertension; RTCSCine, real-time cine imaging with compressed sensing; RTCSCineMoCo, real-time cine imaging combines compressed sensing reconstruction and retrospective fully automated respiratory motion correction; SD, standard deviation; SegBH, segmented acquisition with retrospective electrocardiogram gating and breath-hold.

using RTCSCine. Kito et al (19) compared free-breathing compressed sensing cine and standard breath-hold cine MRI on a 3T MR scanner for LV volume assessment in 63 patients. They found both techniques provided acceptable image quality for LV volumetric analysis (score ≥3) in all patients but free-breathing compressed sensing cine had a significantly lower image quality score than standard breath-hold cine (3.7±0.5 and 4.7±0.5; P<0.0001). In their results, free-breathing compressed sensing cine MRI had a tendency to overestimate LVEDV (124.7 *vs.* 120.5; P=0.37) and LVESV values (48.2 *vs.* 45.3; P=0.11) and significantly underestimated LVM values (79.0 *vs.* 83.8; P=0.0006) compared with standard breath-hold cine. In our results, we also found significant higher LVESV values (59.0±38.0 *vs.* 56.5±36.4; P<0.001) and lower LVM values (85.8±33.9 *vs.* 91.2±32.0; P<0.001) derived from RTCSCine than SegBH. These quantitative deviations were perhaps due to the image blur of the RTCSCine mages, resulting in inaccurate LV volumetric assessments. We also observed mildly higher LVEF values (38.9±9.3 *vs.* 37.8±9.1; P=0.010) derived from RTCSCineMoCo in the LVEF <50% subgroup. Patients with reduced LVEF were easier to have difficulty with breath-hold resulting in SegBH image blur, while RTCSCineMoCo could effectively prevent motion artifacts. This might result in the measurement difference and we believed RTCSCineMoCo could be a better technique for patients with reduced LVEF.

We found several studies on myocardial strain analysis using feature tracking in real-time compressed sensing cine CMR. Langton *et al.* (24) firstly used non-rigid registration and real-time highly accelerated cine CMR [4× accelerated, 4-beat/slice (R4), and a 9.2× accelerated 2-beat/slice (R9.2)] to estimate myocardial strain (GCS, and GRS) in 20 healthy volunteers and 20 patients. Compared with conventional 14-beat/slice cine acquisition, there was a significant underestimation of GCS and GRS in R4 and R9.2, but high consistency between conventional acquisition and R4 and between conventional acquisition and R9.2. In our study, SegBH with segmented acquisition acquired the highest strain values, and RTCSCineMoCo that extended real-time data acquisition to multiple heartbeats showed improved performance compared with single-shot RTCSCine, in the myocardial strain analyses. Our study also confirmed that acquisition strategies could influence myocardial global strain values. Chen *et al.* (25) simultaneously evaluated LV function and strain using two-, three-, and four- long-axis and a stack of short-axis cine imaging derived from single-shot compressed sensing CMR in 37 participants. They found significant differences in function parameters including LVESV, LVSV, and LVEF, which was similar to our study, but no difference in LVM. Additionally, they demonstrated that the strain parameters (GLS, GCS, and

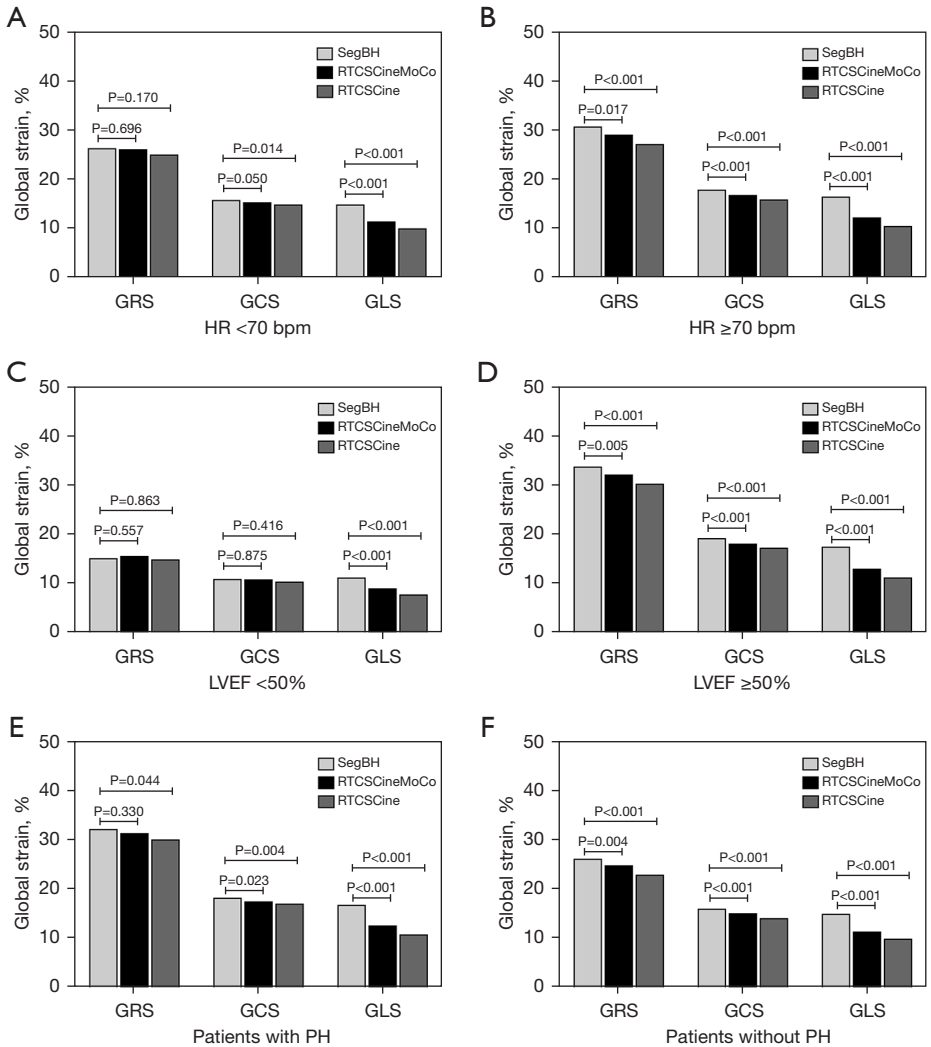

Figure 6 Comparison of global strain in radial (GRS), circumferential (GCS), and longitudinal (GLS) between RTCSCineMoCo and SegBH and between RTCSCine and SegBH in subgroups defined by HR (A,B), LVEF (C,D), and etiology (E,F). LVEF, left ventricular ejection fraction; GCS, global circumferential strain; GLS, global longitudinal strain; GRS, global radial strain; HR, heart rate; PH, pulmonary hypertension; RTCSCine, real-time cine imaging with compressed sensing; RTCSCineMoCo, real-time cine imaging combines compressed sensing reconstruction and retrospective fully automated respiratory motion correction; SegBH, segmented acquisition with retrospective electrocardiogram gating and breath-hold.

GRS) derived from single-shot compressed sensing cine images were significantly lower compared with conventional segmented cine imaging. In our study, as the same as Chen, we combined long- and short-axis images to analyse myocardial strain in a larger cohort (67 patients). We also found strain analyses results by free-breathing compressed sensing techniques were underestimated compared with SegBH, but the absolute global strain values measured by RTCSCineMoCo were closer to the reference SegBH. Yang *et al.* (26) compared GLS, GRS, GCS, and strain rate by breath-hold compressed sensing cine imaging at high temporal resolution (10 ms) and conventional temporal resolution (40 ms) and found that high temporal resolution resulted in significantly higher cardiac strain and strain rate values, particularly for GRS and GCS measured in patients with LVEF ≥50% and HR <70 bpm. Their results suggested that different temporal resolutions of cine imaging, HRs and EFs might all affect the strain analyses measurements.

In our study, RTCSCineMoCo and RTCSCine had varied temporal resolutions (RR interval/25), and SegBH had fixed acquired temporal resolutions [45 ms (interpolated to 25 cardiac phases)]. The strain values derived from RTCSCineMoCo and RTCSCine were lower than SegBH. We also performed subgroup analyses according to HR, LVEF, and etiology. We found that RTCSCineMoCo had a better performance in the lower HR group (HR <70 bpm) and the reduced LVEF group (LVEF <50%) for GRS and GCS analyses, but the GLS values were still underestimated in subgroup analyses. In our primary subgroup analysis based on etiology (patients with or without PH), we found results as similar as in total group. Several studies (27,28) mentioned that the reduced blood-to-myocardium contrast of highly-accelerated compressed sensing acquisition affects delineation of endo- or epi-myocardial contour, resulting in partial myocardial mistracking. This could be the reason for global strain values measurement deviations. In our study, we also observed more prominent location changes and image blurs in long-axis images by free-breathing compressed sensing techniques (both of RTCSCineMoCo and RTCSCine) compared to SegBH, which suggested long-axis images might be affected by respiratory motion more obviously so that the results of GLS.

We also compared TPS using the three cine imaging techniques. TPS is the time from end-diastolic myocardial strain (off-peak) to the peak strain in the radial (TPS_R), circumferential (TPS_C), and longitudinal (TPS_L) directions. All TPS parameters had strong correlations in our study, with no statistical differences between RTCSCineMoCo and SegBH and only a small statistical difference in TPS_L (305.0±55.8 *vs.* 317.4±53.8; P=0.011) between RTCSCine and SegBH. These results illustrated that real-time compressed sensing cine CMR might be a promising tool for analyzing TPS parameters during free-breathing or rapid acquisition.

This study had several limitations. First, we only used one technique for volume and strain analyses; other algorithms might have responded to differences. Second, there are some other LV myocardial strain parameters, such as strain rate, and only a select few were included. Further evaluations including more strain parameters in a larger cohort are warranted to clarify the usefulness of real-time compressed sensing cine CMR imaging for myocardial strain assessments. Third, we performed the three cine techniques sequentially. Randomized scan order would be more optimal to avoid potential bias. Fourth, study on right ventricular function and strain analyses is further needed. Fifth, our study group had heterogeneous etiologies. Further study in patients with homogeneous etiology can reduce confounding factors and make more clinical reference value.

Conclusions

RTCSCineMoCo is a promising method for robust free-breathing cardiac cine imaging with shortened scan time, achieving more precise quantitative analysis results for LV function. RTCSCineMoCo mildly underestimated GRS, GCS, and GLS, but showed smaller bias compared to RTCSCine in LV strain analysis. RTCSCineMoCo is a promising option for subjects who have difficulty holding their breath such as children and those with heart failure or sedated.

Acknowledgments

Funding: This work was supported by the Major International (Regional) Joint Research Project of National Natural Science Foundation of China (Grant No. 82020108018), Beijing Natural Science Foundation (No. Z210013), the National High Level Hospital Clinical Research Funding (No. 2022-PUMCH-A-095), the National High Level Hospital Clinical Research Funding (No. 2022-PUMCH-B-027), and the National High Level Hospital Clinical Research Funding (No. 2022-PUMCH-D-002).

Footnote

Conflicts of Interest: All authors have completed the ICMJE uniform disclosure form (available at https://qims.amegroups.com/article/view/10.21037/qims-22-596/coif). JP is an employee of Siemens Medical Solutions USA Inc., Chicago, IL USA. JA is an employee of Siemens Shenzhen Magnetic Resonance Ltd., Shenzhen, China. The other authors have no conflicts of interest to declare.

Ethical Statement: The authors are accountable for all aspects of the work in ensuring that questions related to the accuracy or integrity of any part of the work are appropriately investigated and resolved. The study was conducted in accordance with the Declaration of Helsinki (as revised in 2013). This study was approved by Institutional Committee of Ethics of Peking Union Medical College Hospital (No.JS-2658). All participants signed written

informed consent before undergoing cardiac MRI scans.

References

1. Xu J, Yang W, Zhao S, Lu M. State-of-the-art myocardial strain by CMR feature tracking: clinical applications and future perspectives. Eur Radiol 2022;32:5424-35.
2. Taylor RJ, Moody WE, Umar F, Edwards NC, Taylor TJ, Stegemann B, Townend JN, Hor KN, Steeds RP, Mazur W, Leyva F. Myocardial strain measurement with feature-tracking cardiovascular magnetic resonance: normal values. Eur Heart J Cardiovasc Imaging 2015;16:871-81.
3. Truong VT, Palmer C, Wolking S, Sheets B, Young M, Ngo TNM, Taylor M, Nagueh SF, Zareba KM, Raman S, Mazur W. Normal left atrial strain and strain rate using cardiac magnetic resonance feature tracking in healthy volunteers. Eur Heart J Cardiovasc Imaging 2020;21:446-53.
4. Reindl M, Tiller C, Holzknecht M, Lechner I, Beck A, Plappert D, Gorzala M, Pamminger M, Mayr A, Klug G, Bauer A, Metzler B, Reinstadler SJ. Prognostic Implications of Global Longitudinal Strain by Feature-Tracking Cardiac Magnetic Resonance in ST-Elevation Myocardial Infarction. Circ Cardiovasc Imaging 2019;12:e009404.
5. Elias J, van Dongen IM, Hoebers LP, Ouweneel DM, Claessen BEPM, Råmunddal T, Laanmets P, Eriksen E, Piek JJ, van der Schaaf RJ, Ioanes D, Nijveldt R, Tijssen JG, Henriques JPS, Hirsch A; . Recovery and prognostic value of myocardial strain in ST-segment elevation myocardial infarction patients with a concurrent chronic total occlusion. Eur Radiol 2020;30:600-8.
6. Chen X, Pan J, Shu J, Zhang X, Ye L, Chen L, Hu Y, Yu R. Prognostic value of regional strain by cardiovascular magnetic resonance feature tracking in hypertrophic cardiomyopathy. Quant Imaging Med Surg 2022;12:627-41.
7. Leng S, Tan RS, Guo J, Chai P, Zhang G, Teo L, Ruan W, Yeo TJ, Zhao X, Allen JC, Tan JL, Yip JW, Chen Y, Zhong L. Cardiovascular magnetic resonance-assessed fast global longitudinal strain parameters add diagnostic and prognostic insights in right ventricular volume and pressure loading disease conditions. J Cardiovasc Magn Reson 2021;23:38.
8. Chen X, Hu H, Pan J, Shu J, Hu Y, Yu R. Performance of cardiovascular magnetic resonance strain in patients with acute myocarditis. Cardiovasc Diagn Ther 2020;10:725-37.
9. McMurray JJ, Adamopoulos S, Anker SD, Auricchio A, Böhm M, Dickstein K, et al. ESC guidelines for the diagnosis and treatment of acute and chronic heart failure 2012: The Task Force for the Diagnosis and Treatment of Acute and Chronic Heart Failure 2012 of the European Society of Cardiology. Developed in collaboration with the Heart Failure Association (HFA) of the ESC. Eur J Heart Fail 2012;14:803-69.
10. Sudarski S, Henzler T, Haubenreisser H, Dösch C, Zenge MO, Schmidt M, Nadar MS, Borggrefe M, Schoenberg SO, Papavassiliu T. Free-breathing Sparse Sampling Cine MR Imaging with Iterative Reconstruction for the Assessment of Left Ventricular Function and Mass at 3.0 T. Radiology 2017;282:74-83.
11. Haubenreisser H, Henzler T, Budjan J, Sudarski S, Zenge MO, Schmidt M, Nadar MS, Borggrefe M, Schoenberg SO, Papavassiliu T. Right Ventricular Imaging in 25 Seconds: Evaluating the Use of Sparse Sampling CINE With Iterative Reconstruction for Volumetric Analysis of the Right Ventricle. Invest Radiol 2016;51:379-86.
12. Basha TA, Akçakaya M, Liew C, Tsao CW, Delling FN, Addae G, Ngo L, Manning WJ, Nezafat R. Clinical performance of high-resolution late gadolinium enhancement imaging with compressed sensing. J Magn Reson Imaging 2017;46:1829-38.
13. Pennig L, Lennartz S, Wagner A, Sokolowski M, Gajzler M, Ney S, Laukamp KR, Persigehl T, Bunck AC, Maintz D, Weiss K, Naehle CP, Doerner J. Clinical application of free-breathing 3D whole heart late gadolinium enhancement cardiovascular magnetic resonance with high isotropic spatial resolution using Compressed SENSE. J Cardiovasc Magn Reson 2020;22:89.
14. Mesropyan N, Isaak A, Dabir D, Hart C, Faron A, Endler C, Kravchenko D, Katemann C, Pieper CC, Kuetting D, Attenberger UI, Luetkens JA. Free-breathing high resolution modified Dixon steady-state angiography with compressed sensing for the assessment of the thoracic vasculature in pediatric patients with congenital heart disease. J Cardiovasc Magn Reson 2021;23:117.
15. Hoyer UCI, Lennartz S, Abdullayev N, Fichter F, Jünger ST, Goertz L, Laukamp KR, Gertz RJ, Grunz

JP, Hohmann C, Maintz D, Persigehl T, Kabbasch C, Borggrefe J, Weiss K, Pennig L. Imaging of the extracranial internal carotid artery in acute ischemic stroke: assessment of stenosis, plaques, and image quality using relaxation-enhanced angiography without contrast and triggering (REACT). Quant Imaging Med Surg 2022;12:3640-54.
16. Camargo GC, Erthal F, Sabioni L, Penna F, Strecker R, Schmidt M, Zenge MO, Lima RS, Gottlieb I. Real-time cardiac magnetic resonance cine imaging with sparse sampling and iterative reconstruction for left-ventricular measures: Comparison with gold-standard segmented steady-state free precession. Magn Reson Imaging 2017;38:138-44.
17. Lin ACW, Strugnell W, Riley R, Schmitt B, Zenge M, Schmidt M, Morris NR, Hamilton-Craig C. Higher resolution cine imaging with compressed sensing for accelerated clinical left ventricular evaluation. J Magn Reson Imaging 2017;45:1693-9.
18. Pang J, Leon PI, Bi X, McNeal G, Forman C, Leidecker C, Masand PM. Free-Breathing Cardiac Cine MRI with Compressed Sensing Real-Time Imaging and Retrospective Motion Correction. ISMRM 2020:abstract 2190. Available online: https://www.ismrm.org/20/program_files/DP02-02.htm#006 (accessed on 6/3/2022).
19. Kido T, Kido T, Nakamura M, Watanabe K, Schmidt M, Forman C, Mochizuki T. Assessment of Left Ventricular Function and Mass on Free-Breathing Compressed Sensing Real-Time Cine Imaging. Circ J 2017;81:1463-8.
20. Rahsepar AA, Saybasili H, Ghasemiesfe A, Dolan RS, Shehata ML, Botelho MP, Markl M, Spottiswoode B, Collins JD, Carr JC. Motion-Corrected Real-Time Cine Magnetic Resonance Imaging of the Heart: Initial Clinical Experience. Invest Radiol 2018;53:35-44.
21. Schulz-Menger J, Bluemke DA, Bremerich J, Flamm SD, Fogel MA, Friedrich MG, Kim RJ, von Knobelsdorff-Brenkenhoff F, Kramer CM, Pennell DJ, Plein S, Nagel E. Standardized image interpretation and post-processing in cardiovascular magnetic resonance - 2020 update : Society for Cardiovascular Magnetic Resonance (SCMR): Board of Trustees Task Force on Standardized Post-Processing. J Cardiovasc Magn Reson 2020;22:19.
22. Vincenti G, Monney P, Chaptinel J, Rutz T, Coppo S, Zenge MO, Schmidt M, Nadar MS, Piccini D, Chèvre P, Stuber M, Schwitter J. Compressed sensing single-breath-hold CMR for fast quantification of LV function, volumes, and mass. JACC Cardiovasc Imaging 2014;7:882-92.
23. Goebel J, Nensa F, Schemuth HP, Maderwald S, Quick HH, Schlosser T, Nassenstein K. Real-time SPARSE-SENSE cine MR imaging in atrial fibrillation: a feasibility study. Acta Radiol 2017;58:922-8.
24. Langton JE, Lam HI, Cowan BR, Occleshaw CJ, Gabriel R, Lowe B, Lydiard S, Greiser A, Schmidt M, Young AA. Estimation of myocardial strain from non-rigid registration and highly accelerated cine CMR. Int J Cardiovasc Imaging 2017;33:101-7.
25. Chen Y, Qian W, Liu W, Zhu Y, Zhou X, Xu Y, Zhu X. Feasibility of single-shot compressed sensing cine imaging for analysis of left ventricular function and strain in cardiac MRI. Clin Radiol 2021;76:471.e1-7.
26. Yang W, Li H, He J, Yin G, An J, Forman C, Schmidt M, Zhao S, Lu M. Left Ventricular Strain Measurements Derived from MR Feature Tracking: A Head-to-Head Comparison of a Higher Temporal Resolution Method With a Conventional Method. J Magn Reson Imaging 2022;56:801-11.
27. Kido T, Hirai K, Ogawa R, Tanabe Y, Nakamura M, Kawaguchi N, Kurata A, Watanabe K, Schmidt M, Forman C, Mochizuki T, Kido T. Comparison between conventional and compressed sensing cine cardiovascular magnetic resonance for feature tracking global circumferential strain assessment. J Cardiovasc Magn Reson 2021;23:10.
28. Goebel J, Nensa F, Bomas B, Schemuth HP, Maderwald S, Gratz M, Quick HH, Schlosser T, Nassenstein K. Real-time SPARSE-SENSE cardiac cine MR imaging: optimization of image reconstruction and sequence validation. Eur Radiol 2016;26:4482-9.

Cite this article as: Li Y, Lin L, Wang J, Cao L, Liu Y, Pang J, An J, Jin Z, Wang Y. Cardiac cine with compressed sensing real-time imaging and retrospective motion correction for free-breathing assessment of left ventricular function and strain in clinical practice. Quant Imaging Med Surg 2023;13(4):2262-2277. doi: 10.21037/qims-22-596

